HERA-19 Commissioning: Results from Sky Calibration
HERA Memorandum Number 23
March 17, 2017

C.L. Carilli[1,2], B. Nikolic[2], K. Gale-Sides[2]

ccarilli@aoc.nrao.edu

ABSTRACT

We present results from sky calibration procedures using the Galactic Center (GC) as a calibrator, for HERA19 data from June 2016. We find that the antenna-based delays and mean phase offsets are stable to a few percent on timescales of days. We also find that these quantities are robust to employing a point source vs. a CLEAN calibration model, to similar accuracy. The GC can be used to calibrate for about ±30min around transit. The complex antenna-based bandpass solutions do show significant changes from a point source to a CLEAN model, indicating that the intrinsic structure of the GC must be included in the BP calibration process. The bandpass solutions converge with 2 iterations of imaging and self-calibration, to within a few degrees and a few percent in phase and amplitude, and the BP solutions repeat from day to day to a similar level. We apply calibration solutions from the GC to other times, including when Centaurus A is transiting, and a high latitude field. Known sources are recovered (eg. Cen A), and the sky structure reproduces from day to day consistently. We track the peak amplitude of the GC in images through transit to get an estimate of the primary beam response, at least along the cut that the GC follows (1.63^o from zenith). We find a FWHM for the beam cut of 12.6^o averaging over the full band, and 13.5^o for the lower part of the band (channels < 400 or frequencies below 141MHz), and 11.0^o for the upper part of the band.

---

[1]National Radio Astronomy Observatory, P. O. Box 0, Socorro, NM 87801

[2]Cavendish laboratory, Cambridge University, UK

1. Data and Processing

This is the third in a series of memos analyzing HERA-19 data frmo 2016. The first investigated closure quantities and dispersion between antennas, without considering calibration (Carilli 2016). The second demonstrated the methods and viability of sky calibration using the Galactic Center (GC), starting from a point source model for delay calibration. The GC transits within 1.63^o of zenith. In this memo, we investigate in more detail the calibration solutions as a function of time, and apply these solutions to other times in order image the sky.

We analyze data from June 2016 for the HERA-19 array. The array and data format (bandwidth, channel width, time resolution), are desribed in Carilli (2016). The data were converted to CASA measurement sets using processes described in Nikolic et al. (2016). Flagging by channel was applied based on visual inspection of visibility spectra, and known bad antennas were flagged, leaving 17 antennas total.

The sky calibration process is described in detail in Nikolic et al. (2016). In brief, after flagging, the antenna based delays are derived using the 'K' solution option in gaincal in CASA, and using a point source model for the GC. This process removes the significant phase slopes as a function of frequency seen in the measured visibilities, effectively removing any phase wraps over the band. A second gaincal is then run to determine the mean phase offset across the band for each antenna.

The resulting data set is then imaged with CLEAN to produce a CLEAN component model of the extended emission across the GC. This CLEAN model is than used to determine the complex bandpasses of the antennas (amplitude and phase versus frequency). A second iteration is performed, leading to the final bandpasses.

We then apply the resulting calibration (delays, mean phase offsets, bandpasses) to the GC itself, and to data taken at other times of day.

2. Results

2.1. Delays

We have calibrated six days worth of data from June 2016. Figure 1a shows the delay solutions for the 6 days for each antenna. The delay solutions are stable day to day to within a few percent. We have performed a similar test of the mean phase offsets, and find stability to within a few degrees day to day.

Figure 1b shows the delays derived for a series of 10min scans over the course of transit of the GC on one day (about 2hrs total). We find that good delay solutions can be derived within ±30min of transit, beyond which the primary beam attenuation lowers the signal enough that the source is lost.

Figure 2 plots the delays derived using a point source model vs. those derived using a CLEAN model from further calibration below. We find small changes with model complexity for the delays, again to a few percent. Note that any residual bandpass structure after delay and mean phase calibration assuming a point source model, will be taken out with the subsequent bandpass calibration. The erlevant quantity is the product of the two calibration steps.

2.2. Bandpasses

Figure 3 shows the bandpass solutions using a model derived from two iterations of self-calibration on the GC, starting with data to which delay and mean phase calibration was applied. The amplitudes range over ±20%, while the phases show structure of $\pm 20^o$. We find that the solutions converge quickly, to within a few percent and a few degrees, in two iterations of self-cal. We find similar bandpass solutions on consecutive days, again to within a few percent and a few degrees.

The question arises: does the bandpass structure reflect the true complex gain response of the system, or is there residual structure due to a non-perfect GC sky model? The rapid convergence and consistency day to day suggest that most of the observed structure is the resonse of the system, and not model limitations. A similar argument can be made from the fact that real sky structure is observed after calibration (see section 2.3). However, none of these arguments is conclusive, and further tests are required to determine the contribution of residual model errors to the derived bandpasses.

2.3. Imaging applications

Figure 4a shows the image of the GC made after calibration. We employ Briggs weighting with Robust = 0.5, plus multifrequency synthesis over the full band, and a multiscale clean. A clean region is set, centered on the primary beam with a radius of 9^o. The dynamic range in this image is about 250 (peak surface brightness/rms noise). The PSF FWHM = 1.4^o. PSF plots for different visibility weighting can be found in Nikolic et al. (2016). Note that residual grating lobes are apparent at about 9^o from the GC itself.

Figures 4b,c show the GC image made from the low and the high frequency parts of the band (below and above channel 400 = 141MHz). The structures in the images are similar, with more extended emission seen at lower frequency. The PSF FWHM in the lower frequency image is 1.65^o, while that in the upper half is 1.25^o.

We then apply the GC calibration solutions to data at other times. Figure 5 shows two images at the LST during which Centaurus A transits. Centaurus A is centered at -43^o declination, and has a total extent at low frequency of about 7^o, in the North-South direction. Centaurus A is seen clearly south of the main beam of the telescope. Figure 5a shows the image made from data taken on the same day as the GC calibration being used. Figure 5b shows an image made applying the same GC calibration to the following day. The images are very similar, supporting the conclusion that the structure being observed is real sky structure.

Note that the structure includes both positive and negative structure: at these low frequencies and short baselines, the visibilities can be dominated by diffuse emission. Hence, without total power information, the resulting images will have both negative and postive structures that reflect the true sky brightness in some convoluted manner (see Carilli & Sims 2016).

Figure 6 shows the resulting image at a relatively high Galactic latitude (22HR LST). Images on two different days again show almost identical structure, suggesting real sky structure is being recovered.

2.4. GC through transit

Figure 7 shows the amplitude of the peak of the GC for a series of images made as over transit. Note that the GC passes 1.63^o from zenith for the HERA antennas.

Three cuts are shown, all normalized to a peak of unity. The blue curve is for images made averaging data over the full band. The red curve is for images made using only the low channels (below channel 400 or about 141MHz), and the green is for channels above 400. We find a FWHM for the beam cut of 12.6^o averaging over the full band, 13.5^o for the lower part of the band, and 11.0^o for the upper part of the band.

In a future memo we will compare these beam cuts to the beam models of de Lera Acedo.

3. Summary

We present results from sky calibration procedures using the Galactic Center (GC) as a calibrator. The main conclusions of the work thus far are:

- The antenna-based delays and mean phases offsets are stable to a few percent on timescales of days.
- The delays and phase offsets are robust to employing a point source vs. a CLEAN calibration model, again to a few percent.
- The GC can be used as a calibrator for about ±30min around transit.
- The antenna-based bandpass solutions do show significant changes from a point source to a CLEAN model. These solutions converge within 2 iterations of imaging and self-calibration, to within a few degrees and a few percent in phase and amplitude. The BP solutions repeat from day to day to a similar level.
- The GC sky calibration solutions, and overall gain stability, allow for application of the solutions over daily timescales, resulting in good images of the sky, with known sources identified (eg. Cen A).
- We track the GC amplitude through transit. The results imply a FWHM for this cut through the primary beam (1.63^o from zenith) of $\sim 12.6^o$ averaging over the full bandwidth. The values for the FWHM for the lower and upper part of the band (channels below/above 400), are: $\sim 13.5^o$ and $\sim 11.0^o$, respectively.

Overall, sky calibration solutions are very stable, and application on daily timescales is reasonable, at least to a few percent accuracy. However, the question remains as to what part of the bandpass structure might still relate to incompleteness in the CLEAN model for the GC. We are considering tests that might address this important question.

References

Nikolic, B., Carilli, C., & Sims, P. 2016, HERA memo 22 (http://reionization.org/science/memos/)

Carilli, C. 2016, HERA memo 15 (http://reionization.org/science/memos/)

Carilli, C., & Sims, P. 2016, HERA memo 12 (http://reionization.org/science/memos/)

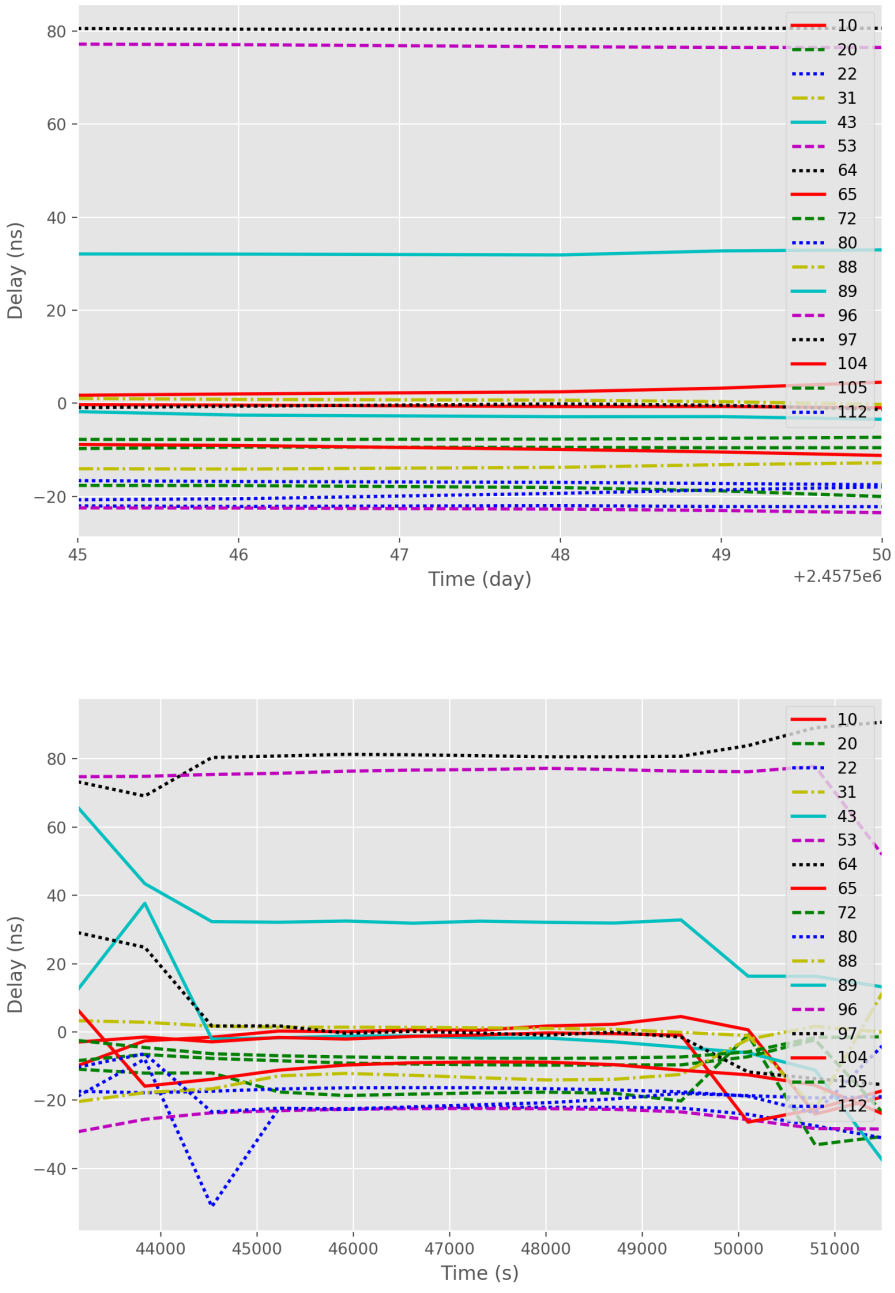

Fig. 1.— Top: Delays derived from gaincal assuming a point source model for the GC for 6 days of HERA19 data. Bottom: Delays over about two hours of time while the GC is transiting.

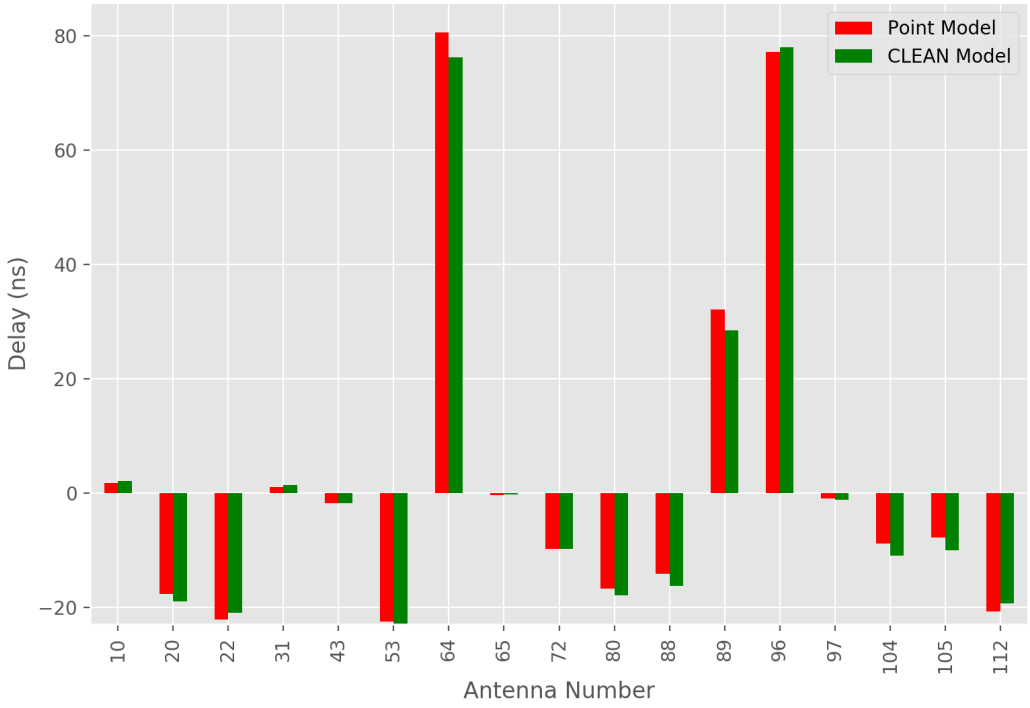

Fig. 2.— Delays derived from gaincal assuming a point source model for the GC versus delays derived using a CLEAN model after further bandpass calibration and imaging, as a function of CASA antenna number.

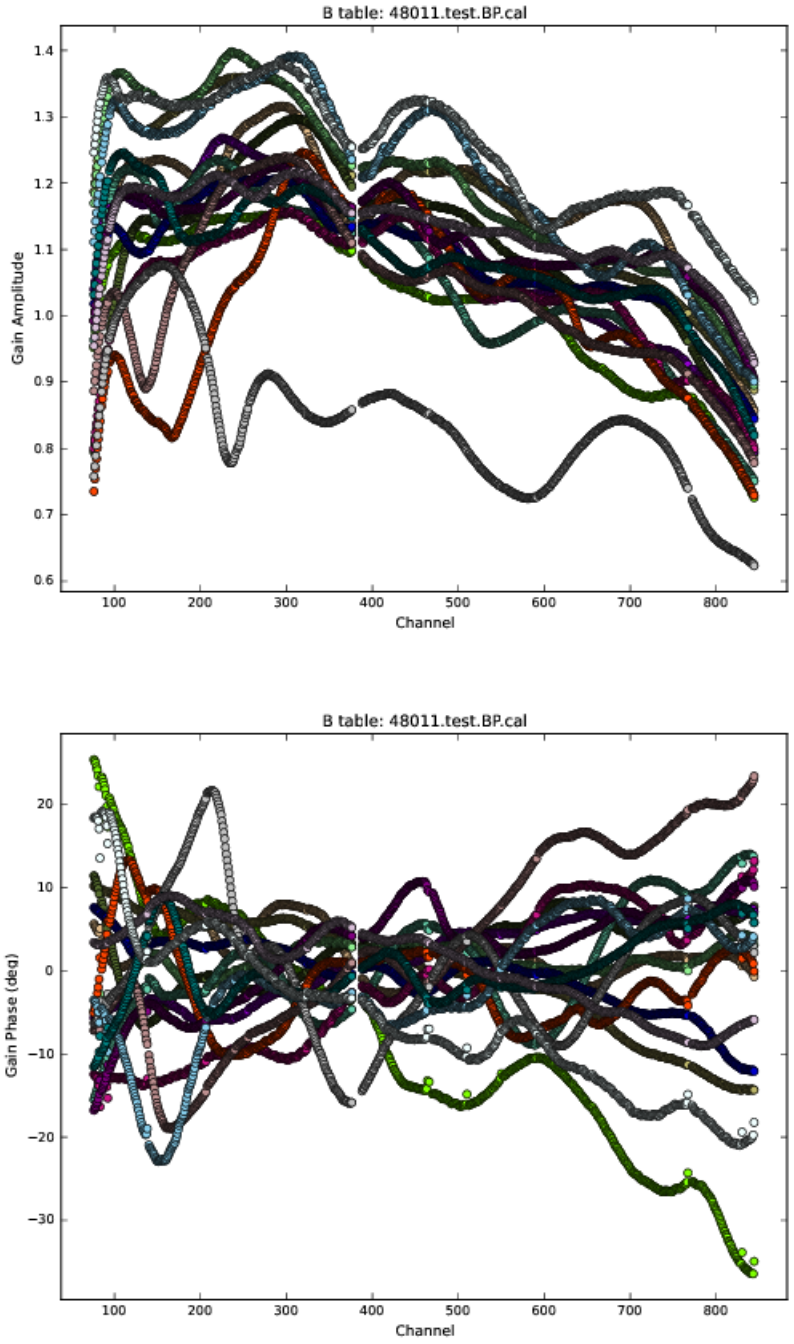

Fig. 3.— Final bandpass solutions using a model derived from two iterations of self-calibration and imaging of the GC. Top: amplitudes. Bottom: phases.

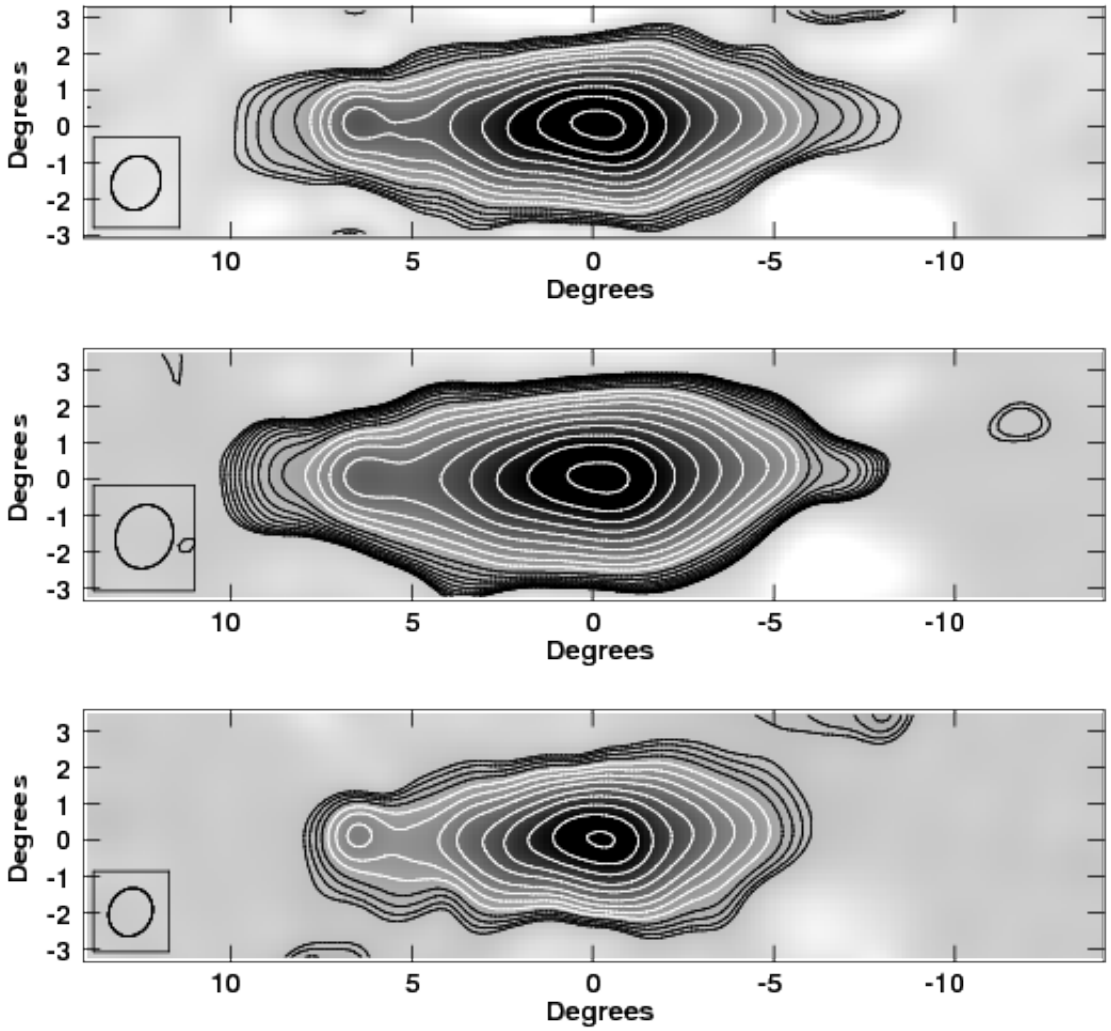

Fig. 4.— Top: Image of the Galactic Center over the full frequency range. The synthesized beam FWHM = 1.4^o. Contour levels are geometric progress ion square root two. Middle: Image of the GC using the lower half of the band, with a FWHM = 1.65^o. Bottom: image of the GC using the upper half of the band, with a FWHM = 1.25^o.

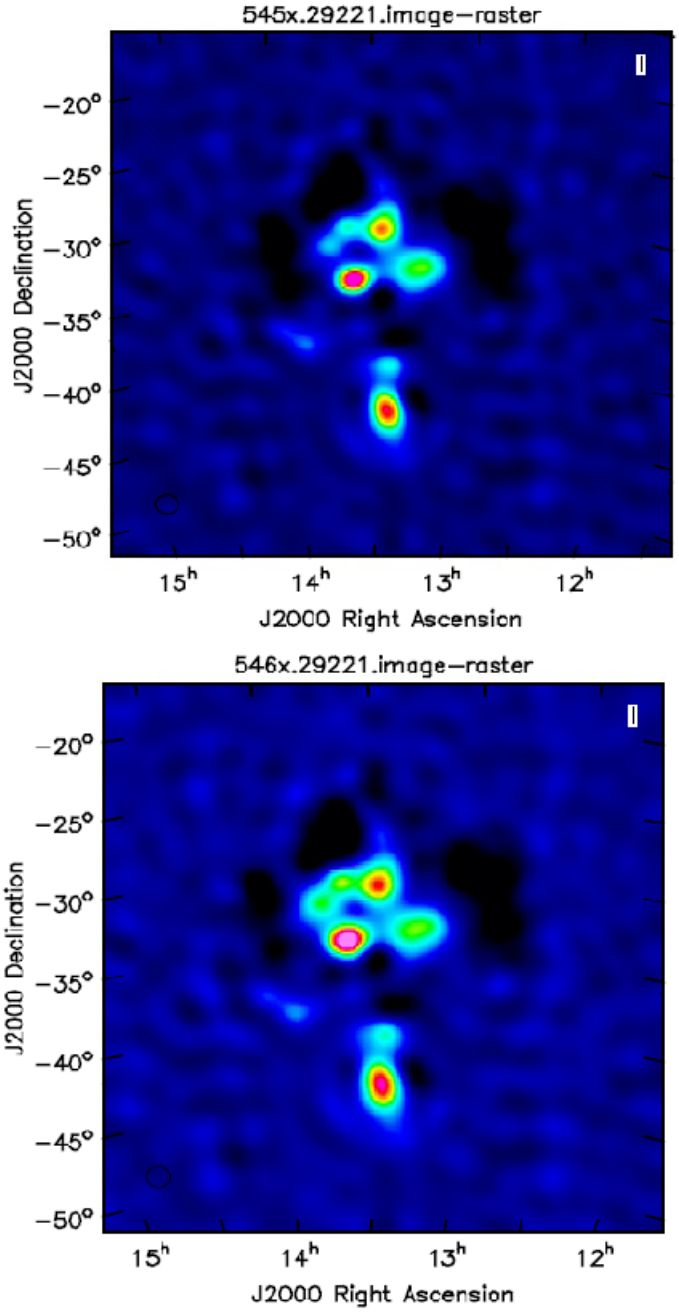

Fig. 5.— Top: Image of the Centaurus A transit time on day 1. Bottom: same, but for day 2 with day 1 GC calibration applied. Centaurus A is the extended source in the south.

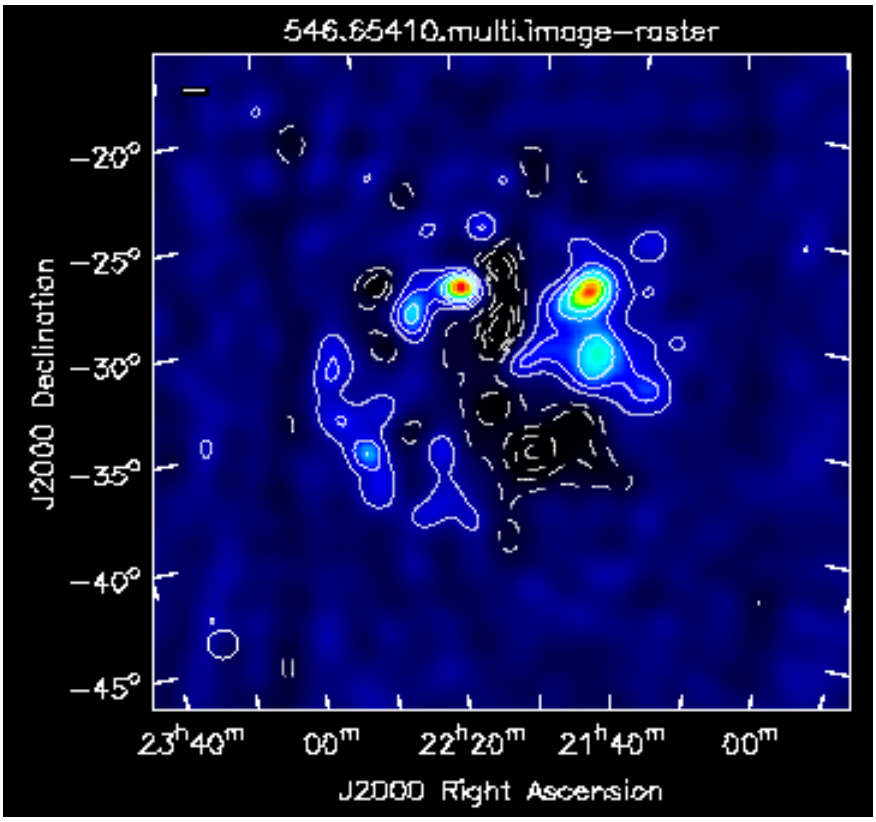

Fig. 6.— Image of a high Galactic latiture field (LST 22hr).

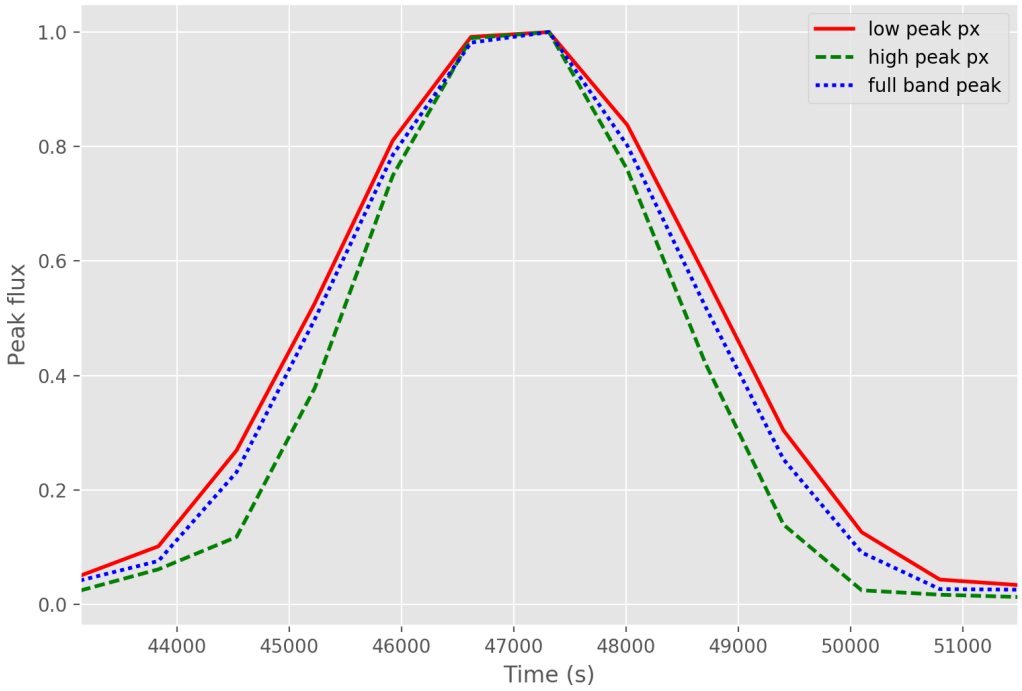

Fig. 7.— Blue: Peak surface brightness of the GC versus time over transit for the full band. Red: same, but for the low half of the band. Green: same, but for the high part of the band.